Electronic Supplementary Information

Amorphous Fe-O-P electro(pre)catalysts for energy-efficient H_2 production coupled with ethylene glycol oxidation

Feifei Yuan,[a, c] Xiaoli Chen,[a] Wenhui Yang,[a] Wanting Wu,[a] Manjie Zheng,[a] Jun Xu,*[b] Nan Yu,*[c] and Liyong Chen*[a, d]

a. Department of Pharmaceutical Engineering, Bengbu Medical University, Bengbu, 233030, China. E-mail: lychen@bbmc.edu.cn.
b. Department of Physics, Research Institute for Biomimetics and Soft Matter, Fujian Provincial Key Laboratory for Soft Functional Materials, Xiamen University, Xiamen, 361005 China. E-mail: xujun@xmu.edu.cn.
c. Anhui Laboratory of Molecule-Based Materials, College of Chemistry and Materials Science, Anhui Normal University, Wuhu, 241002, China. E-mail: yn2009@ahnu.edu.cn.
d. Anhui Provincial Key Laboratory of Tumor Evolution and Intelligent Diagnosis and Treatment, Bengbu medical university.

1. Experimental section

1.1 Chemicals and Materials

Fumaric acid ($C_4H_4O_4$, AR, 99.5%), iron nitrate nonahydrate ($Fe(NO_3)_3·9H_2O$, AR, 98.5%), sodium hypophosphite monohydrate ($NaH_2PO_2·H_2O$, AR, 99%), potassium hydroxide (KOH, AR, 95%), ethylene glycol ($C_2H_6O_2$, EG, GC, >99%), platinum on carbon (20% Pt/C) and ruthenium dioxide (RuO_2) were purchased from Macklin Biochemical Co., Ltd. Anhydrous ethanol (CH_3CH_2OH, AR, 99.7%), N, N-Dimethylformamide (C_3H_7NO, DMF, 99%) were purchased from Sinopharm Group Chemical Reagent Co.,Ltd. All reagents and chemicals were used without further purification. Deionized water was used throughout the experiments.

1.2 Synthesis of spindle-shaped Fe-MOF (MIL-88A) microstructures

The spindle-shaped Fe-MOF (MIL-88A) microstructures were prepared following a previously reported method with minor modifications. Typically, 139.6 mg (1.20 mmol) of $C_4H_4O_4$ and 262.6 mg (0.65 mmol) of $Fe(NO_3)_3·9H_2O$ were dissolved in 25 mL of deionized water under magnetic stirring to form a homogeneous solution. After continuously stirring for 30 min at room temperature, the solution was transferred into a 50 mL Teflon-lined stainless steel autoclave and heated at 110 °C for 6 h. Subsequently, the system was allowed to cool naturally to room temperature. The saffron-yellow precipitates were washed several times with deionized water and absolute ethanol to remove impurities, and dried under vacuum at 60 °C for 12 h.

1.3 Synthesis of hollow spindle-shaped amorphous Fe-O-P microstructures

In a typical experiment, hollow spindle-shaped amorphous Fe-O-P microstructures ere synthesized as follows: 50 mg of the as-prepared Fe-MOF was added to a pre-prepared $NaH_2PO_2·H_2O$ (1.5 mmol, 159 mg) in 10 mL of deionized water in a single neck flask. Subsequently, 5 mL of DMF was added into the mixture. The resulting system was ultrasonically treated for 15 min to form a homogeneous suspension. The suspension was then stirred slowly at a reflux temperature of 120 °C for 1 h. Afterward, the saffron-yellow precipitates were collected, washed several times with deionized water and absolute ethanol to remove impurities, and finally dried under vacuum at 60 °C for 12 h. The hollow spindle-shaped Fe-O-P microstructures were thus prepared.

1.4 Characterization

X-ray Diffraction Spectrometry (XRD, Bruker D8 ADVANCE) with Cu Kα radiation was employed for phase analyses of the products. Field emission scanning electron microscopy (FE-SEM) images were obtained using a Hitachi Regulus 8100. Transmission electron microscopy (TEM) images were obtained using a Hitachi HT7700. Fourier transform infrared (FT-IR) spectra were recorded on a Thermo Scientific NICOLET iS50 spectrometer. High-resolution TEM (HRTEM) images, selected area electron diffraction (SAED) patterns, and elemental mapping images were conducted with aberration-corrected high-angle annular dark-field scanning transmission electron microscopy (HAADF-STEM) on an FEI tecnai F20. X-ray

photoelectron spectroscopy (XPS) was conducted using a Thermo Fisher Scientific Escalab 250Xi spectrometer.

1.6 Preparation of working electrodes

To prepare the electrode modified by various samples, a piece of Ni foam (NF, 1 × 1 cm^2) was ultrasonically washed in ethanol and deionized water for 30 min each. Simutaneously, various electrocatalyst inks were prepared by dispersing 5.0 mg of electrocatalyst powder into a mixed solvent, containing 50 μL of Nafion solution (5 wt.%), 450 μL of ethanol, and 500 μL of deionized water under the ultrasonic assistance. After ultrasonic treatment for another 30 min, 500 μL of electrocatalyst ink was dropped on the NF, achieving an electrocatalyst loading of ~2.5 mg cm^{-2}. The resulting working electrodes were dried under vacuum at 60 °C for 12 h. In addition, the NF-supported RuO_2 and the NF-supported Pt/C electrodes were prepared using a similar method.

1.7 Electrochemical measurements

All electrochemical measurements were performed on a CHI 760E electrochemical workstation (CH Instruments, Inc., Shanghai, China) with a standard three-electrode system. The system consisted of NF-supported catalysts as the working electrode, a platinum wire as the counter electrode, and an Hg/HgO electrode as the reference electrode. In all measurements, the reference electrode was calibrated to the reversible hydrogen electrode (RHE) scale in 1.0 M KOH according to the following equation: E(RHE) = E(Hg/HgO) + 0.927 V. Linear sweep voltammetry (LSV) was conducted in 1.0 M KOH solution at a scan rate of 5.0 mV s^{-1} with 90% iR-compensation unless otherwise mentioned. The electrochemical impedance spectroscopy (EIS) measurements were performed over a frequency range of 10^5 to 10^{-2} Hz with a sinusoidal voltage amplitude of 5 mV. Chronopotentiometric curves were recorded for 86 h continuously at a constant current density without iR-compensation. Electrochemical active surface areas (ECSA) were determined from double-layer capacitances (C_{dl}), according to the formula: ECSA = C_{dl}/C_s, where C_s, the specific capacitance, was assumed to be 0.04 mF cm^{-2} in the alkaline solution. C_{dl} was measured through cyclic voltammetry in the non-faradic potential region at scan rates of 30, 60, 90, 120, 150 and 180 mV s^{-1}, respectively. The Δj (j_{anode} - $j_{cathode}$) was calculated at 0.892 V vs RHE for each scan rate, and the resulting Δj/2 was plotted against scan rates. The slope of the resulting line was was used to determine C_{dl}.

1.8 Product Analysis.

The products of ethylene glycol oxidation reaction (EGOR) obtained from the alkaline electrolyte were detected by high-performance liquid chromatography (HPLC, DGU-20A3R, Shimadzu) equipped with an Xtimate Sugar-H column (300 × 7.8 × 5 μm) and a UV detector operating at 210 nm. The column was maintained at a temperature of 35 ℃. A 5 mM aqueous solution of H_2SO_4 was used as the mobile phase with a flow rate of 0.6 mL/min. Specifically, the electrolyte was collected and diluted twice with a 5 mM H_2SO_4 aqueous solution. A 10 μL sampling loop was used. The Faraday efficiency (FE) of oxidation products was calculated using the following equation (1):

$$The\ Faraday\ efficiency\ (\%) = \frac{n \times F \times moles\ of\ product}{total\ charge} \quad (1)$$

where F is the Faraday constant (96485 C mol^{-1}) and n is the number of electrons involved in the formation of each product from ethylene glycol (for example, n = 3 for formic acid) according to the following equation (2).

$$\mathbf{C_2H_6O_2 + 6OH^- \rightarrow 2HCOOH + 4H_2O + 6e^-} \qquad (2)$$

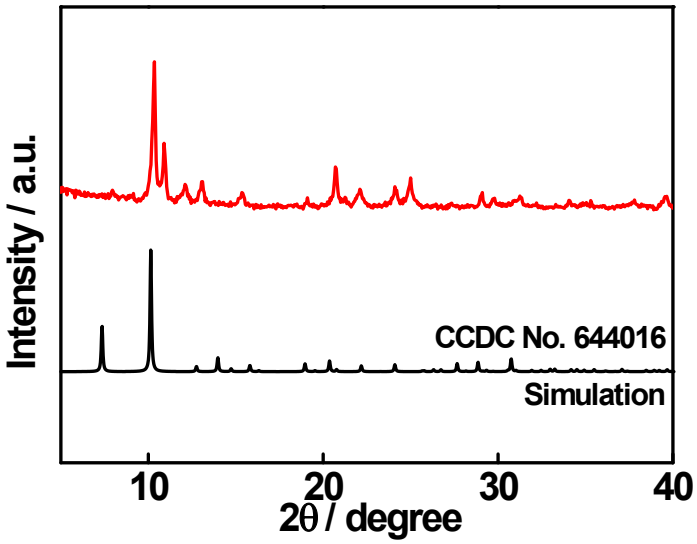

Figure S1. XRD pattern of the as-synthesized MIL-88(A) (red plot).

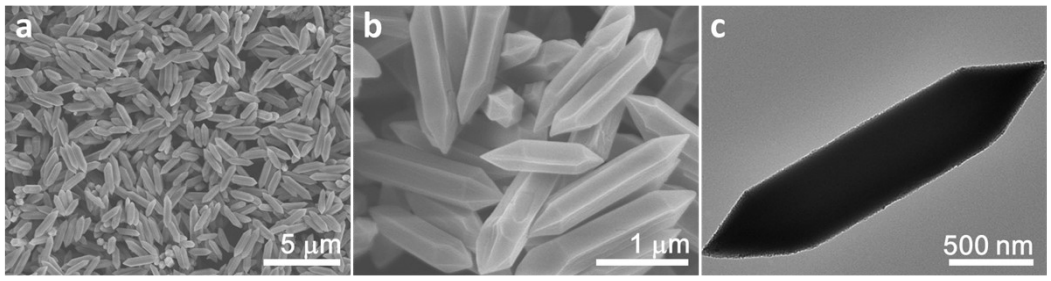

Figure S2. (a) Low-magnification and (b) high-magnification FE-SEM images and (c) TEM image of MIL-88(A).

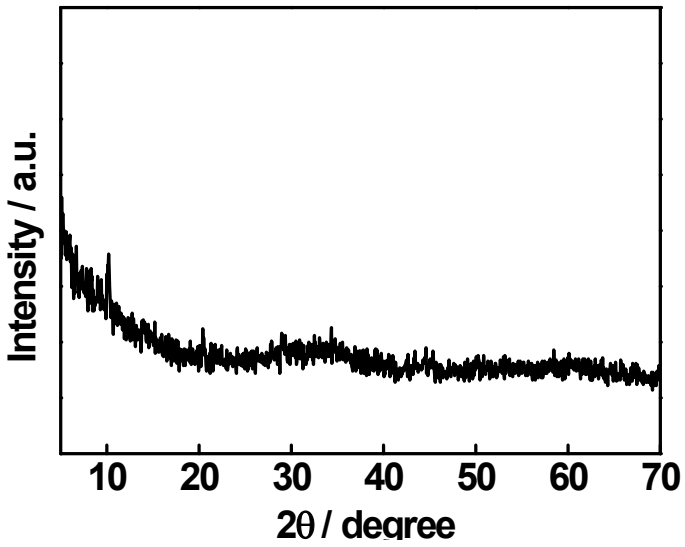

Figure S3. XRD pattern of the as-prepared a-Fe-O-P

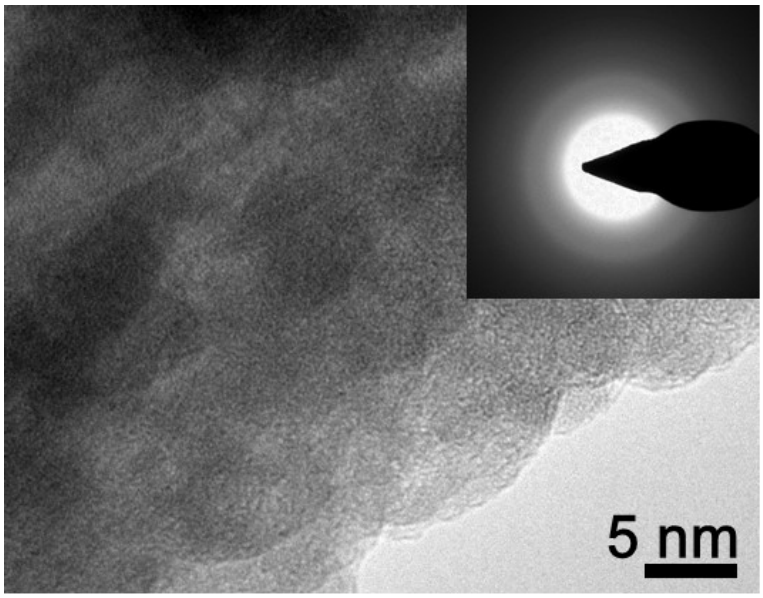

Figure S4. HRTEM image of a-Fe-O-P. Inset is corresponding SAED pattern.

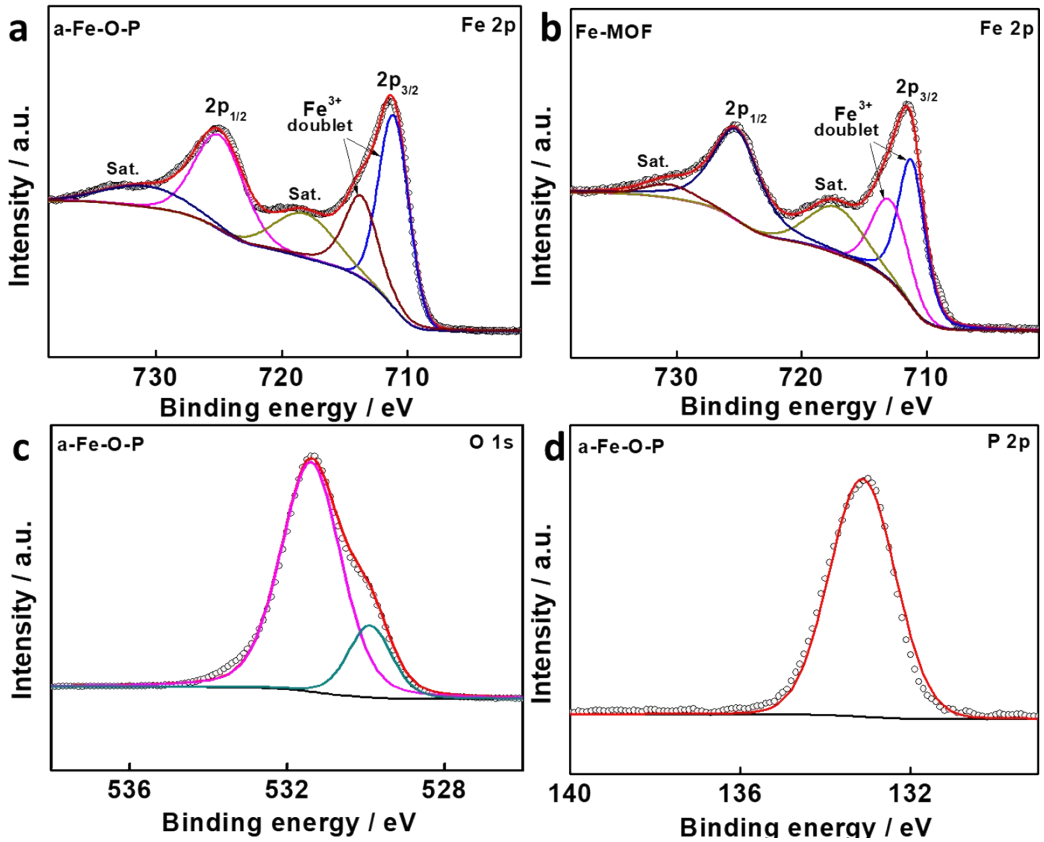

Figure S5. High-resolution XPS spectra of Fe 2p of (a) a-Fe-O-P and (b) Fe-MOF, (c) O 1s and (d) P 2p of a-Fe-O-P.

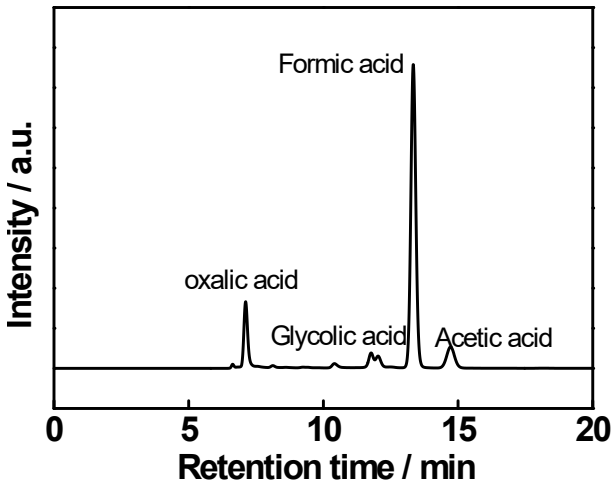

Figure S6. HPLC spectrum of anodic products in the KOH-EG mixed solution after continuous electrocatalysis for 12 h.

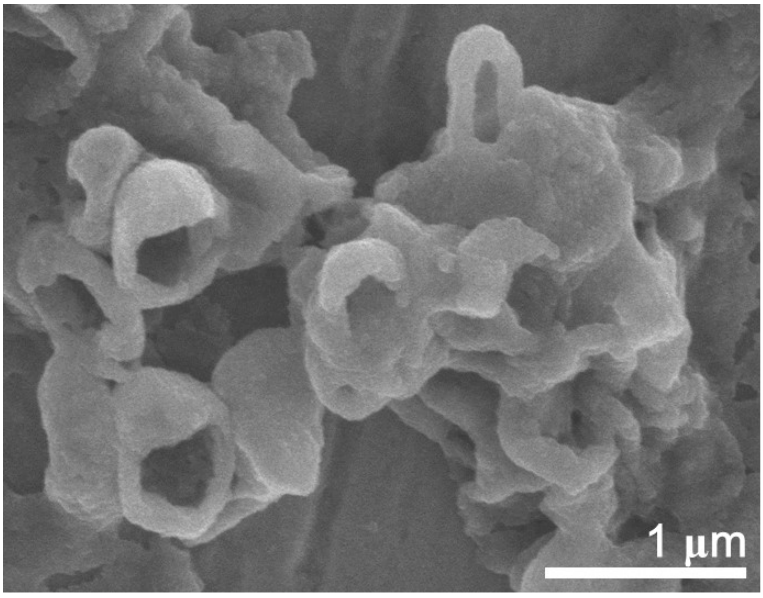

Figure S7. SEM image of a-Fe-O-P after durability test in the KOH-EG electrolyte over 36 h.

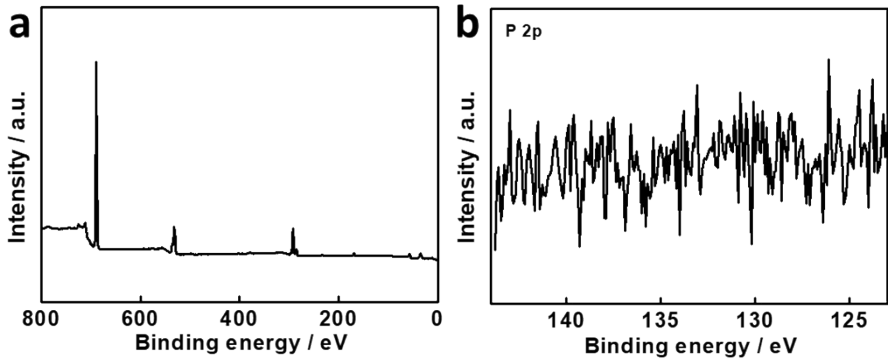

Figure S8. (a) A survey XPS spectrum of a-Fe-O-P after durability test in the KOH-EG electrolyte over 36 h and (b) high-resolution P 2p XPS spectrum.

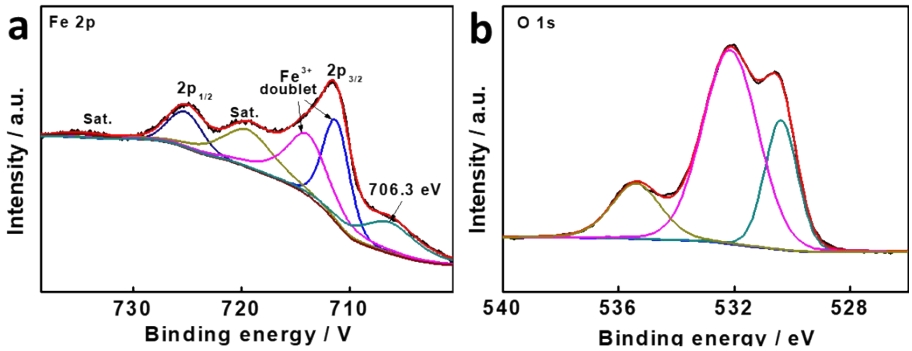

Figure S9. High-resolution XPS spectra of (a) Fe 2p and (b) O 1s of a-Fe-O-P after durability test.

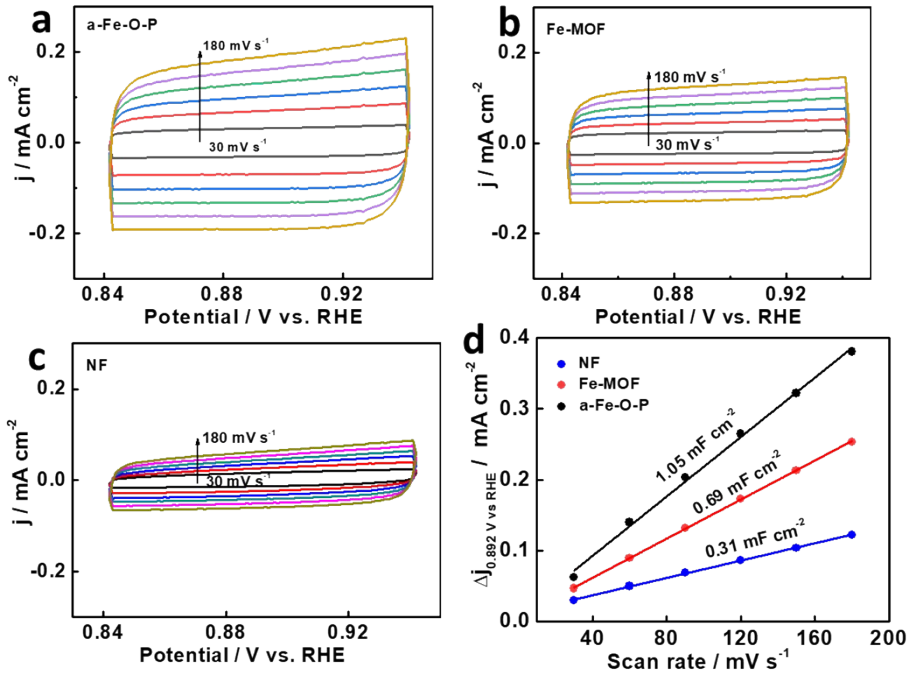

Figure S10. CV curves for various working electrodes of (a) a-Fe-O-P, (b) Fe-MOF, and (c) NF recorded within the potential window of 0.842−0.942 V vs. RHE at different scan rates; (d) the capacitive current densities of electrodes plotted as a function of scan rates from CV curves at 0.892 V vs RHE.

Table S1. Comparison of the electrocatalytic performance of various reported OER electrocatalysts in 1.0 M KOH solution.

Electrocatalysts	Substrate	Current Density / mA cm^{-2}	Overpotential / mV	Stability / h	Ref.
a-Fe-O-P	Ni foam	10 50 100 200	271 304 326 338	86	This work
$FePO_4$ nanosheets	Ni foam	10 100	310 490	15	1
FeP-FeP_xO_y	Glassy carbon	10	280	42	2
V-Fe_2/$FePO_4$	Ni foam	10	270	24	3
CoFe-P	Glassy carbon	10	293	30	4
CoFe@PN-CF	Glassy carbon	10 100	320 400	20	5
$Ni_{0.75}Fe_{0.25}$-P/PO_3@fCNTs	Glassy carbon	10	290	200	6
$NixFe_{1-x}P$	Ni foam	100	340	25	7
amorphous FeCo-PO_x	Carbon paper	10	270	100	8
CoPO	Ni foam	10 200	290 750	10	9
NiCoPO/NC nanosheets	Glassy carbon	10	300	10	10

Reference

1. L. Yang, Z. Guo, J. Huang, Y. Xi, R. Gao, G. Su, W. Wang, L. Cao and B. Dong, *Adv. Mater.*, **29**, 1704574
2. J. Xu, D. Xiong, I. Amorim and L. Liu, *ACS Appl. Nano Mater.*, 2018, **1**, 617-624.
3. P. Ngo, T. Nguyen, M. Singh, R. Balaji, N. Kim and J. Lee, *Appl. Catal., B*, 2023, **331**, 122674.
4. P. Li, W. Li, R. Chen and Y. Lin, *ACS Sustain. Chem. Eng.*, 2020, **8**, 9206-9216.
5. G. Gebreslase, D. Sebastián, M. Martínez-Huerta, T. Tsoncheva, B. Tsyntsarski, G. Georgiev and M. Lázaro. *Catal. Today.*, 2023, **423**, 113991.
6. C. Huang, Y. Zou, Y. Ye, T. Ouyang, K. Xiao and Z. Liu, *Chem. Commun.*, 2019, **55**, 7687-7690.
7. Q. Han, Y. Luo, J. Li, X. Du, S. Sun, Y. Wang, G. Liu and Z. Chen, *Appl. Catal. B Environ.*, 2022, **304**, 120937.
8. X. Liu, H. Yin, S. Zhang, M. Huang, T. Isimjan, X. Yang, D. Cai, *J. Colloid Interface Sci.*,

2024, **653**, 1379-1387
9. G. Anandhababu, Y. Huang, D. Babu, M. Wu and Y. Wang, *Adv. Funct. Mater.*, 2018, **28**, 1706120.
10. C. Wang, W. Chen, D. Yuan, S. Qian, D. Cai, J. Jiang and S. Zhang, *Nano Energy*, 2020, **69**, 104453,